Relativistic stars in vector-tensor theories

Ryotaro Kase,[1] Masato Minamitsuji,[2] and Shinji Tsujikawa[1]
[1]Department of Physics, Faculty of Science, Tokyo University of Science, 1-3, Kagurazaka, Shinjuku-ku, Tokyo 162-8601, Japan
[2]Centro de Astrofísica e Gravitação—CENTRA, Departamento de Física, Instituto Superior Técnico—IST, Universidade de Lisboa—UL, Av. Rovisco Pais 1, 1049-001 Lisboa, Portugal

(Received 24 November 2017; revised manuscript received 13 February 2018; published 9 April 2018)

We study relativistic star solutions in second-order generalized Proca theories characterized by a $U(1)$-breaking vector field with derivative couplings. In the models with cubic and quartic derivative coupling, the mass and radius of stars become larger than those in general relativity for negative derivative coupling constants. This phenomenon is mostly attributed to the increase of star radius induced by a slower decrease of the matter pressure compared to general relativity. There is a tendency that the relativistic star with a smaller mass is not gravitationally bound for a low central density and hence is dynamically unstable, but that with a larger mass is gravitationally bound. On the other hand, we show that the intrinsic vector-mode couplings give rise to general relativistic solutions with a trivial field profile, so the mass and radius are not modified from those in general relativity.

DOI: 10.1103/PhysRevD.97.084009

I. INTRODUCTION

The increasing evidence of dark sectors in the Universe [1,2] implies that there may be some extra propagating degrees of freedom (DOFs) beyond the realm of general relativity (GR). The new DOFs arising in modified gravitational theories can be potentially harmful as they generally mediate fifth forces with ordinary matter. In the local Universe with a weak gravitational field, however, there are several screening mechanisms of fifth forces known in the literature—such as Vainshtein [3] and chameleon [4] mechanisms. This screening property does not necessarily persist in the regime of strong gravity, reflecting the fact that the behavior of new DOFs can be modified by large nonlinearities in the field equations of motion. The direct detections of gravitational waves by Advanced LIGO and Virgo [5,6] have opened up a new window for testing GR in strong gravity regimes.

Besides black holes (BHs), relativistic stars are also important compact objects which allow one to search possible deviation from GR in strong gravity regimes [7,8]. Especially, neutron stars (NSs) are the representative relativistic stars. Inside a NS, the gravitational force balances the degeneracy pressure of fermions [9]. The properties of NSs, including the mass and radius, depend on the equation of state (EOS) of strong interacting matter, i.e., the relation between the matter pressure and density [10,11]. The microscopic determination of the EOS of NSs from underlying nuclear interactions in an extremely high-density regime remains a challenging theoretical problem.

In modified gravitational theories, the existence of extra propagating DOFs can also influence the properties of relativistic stars. In scalar-tensor theories where a scalar field ϕ has a direct coupling with the Ricci scalar R, the Einstein-frame metric $g_{\mu\nu}$ felt by the matter sector is different from the Jordan-frame metric $\tilde{g}_{\mu\nu}$. The relation of these two metrics can be parametrized by the form $\tilde{g}_{\mu\nu} = A^2(\phi)g_{\mu\nu}$, where $A(\phi)$ is a function of ϕ [12]. Inside a star, the conformal coupling to matter can trigger a tachyonic instability of the scalar field, and spontaneously scalarizes the relativistic star. Damour and Esposito-Farèse [13] showed that such a scalarization, which occurs for the coupling, e.g., $A(\phi) = \exp(\beta\phi^2/2)$ (where β is a constant), significantly modifies the properties of relativistic stars with respect to GR. Such a nontrivial excitation of the scalar field is a consequence of the absence of a no-hair theorem for stars. The scalarization can occur only for $\beta \lesssim -4.35$ [14–16], whereas binary-pulsar observations [17] have set stringent bounds on β, as $\beta \gtrsim -4.5$. For NSs, the existence of EOS-independent relations [18] will be important to resolve the degeneracies between the effects associated with modified gravity and uncertainties in EOSs, and to test modified gravitational theories with future observations of NSs.

In shift-symmetric Horndeski (and beyond Horndeski) theories [19,20] with a minimally coupled matter component, the no-hair theorem for relativistic stars was argued in Ref. [21]. The theorem holds under the same assumptions as those used for proving the no-hair theorem of BHs in shift-symmetric Horndeski theories

[22], with the regularity of metric functions and the scalar field at the center of stars. Thus, as in the case of hairy BH solutions [23–31], nontrivial NS configurations have been studied by violating at least one of those assumptions. For example, there exist relativistic star solutions for a linearly time-dependent scalar field $\phi = qt + \psi(r)$ [32–35]. Relativistic stars for other modified gravitational theories have been extensively studied in Refs. [36–38]. In this paper, we will study relativistic star solutions in generalized Proca theories described by a $U(1)$-breaking vector field with derivative couplings. We show that the star configuration with nontrivial influence of the extra DOFs can be constructed more easily compared to scalar-tensor theories.

The action of generalized Proca theories with second-order equations of motion was first constructed in Refs. [39,40] from the demand of keeping three propagating DOFs besides two tensor polarizations. The theories were further extended [41] to include intrinsic vector-mode couplings with the double dual Riemann tensor $L^{\mu\nu\alpha\beta}$ [42], such that the $U(1)$-invariant interactions derived by Horndeski [43] can be accommodated as a specific case. It is also possible to go beyond the second-order domain by keeping the five propagating DOFs [44,45]. In such (beyond) generalized Proca theories, the derivative interactions can drive the late-time cosmic acceleration [46] with some distinct observational signatures [47,48], while satisfying local gravity constraints in the Solar System [49,50].

In the Einstein-Maxwell theory with a massless vector field, the unique static and spherically symmetric BH solution corresponds to the Reissner-Nordström (RN) metric with mass and electric charge. In the Einstein-Proca theory with a massive vector field described by the Lagrangian $-m^2 A^\mu A_\mu/2$, Bekenstein showed that only the static and spherically symmetric BH solution is given by the Schwarzschild metric without the vector hair [51]. This no-hair theorem cannot be applied to vector-tensor theories with derivative self-interactions and nonminimal couplings to the spacetime curvature. Indeed, it is known that there are a bunch of hairy BH solutions in generalized Proca theories [52–63]. In theories with a nonminimal coupling to the Einstein tensor, $\beta_4 G^{\mu\nu} A_\mu A_\nu$, Chagoya *et al.* [53] derived an exact static and spherically symmetric BH solution for the specific coupling $\beta_4 = 1/4$. This exact BH solution was further extended to asymptotically nonflat solutions [55,58], nonexact solutions for $\beta_4 \neq 1/4$ [57,58], and slowly rotating solutions [55]. There are also exact BH solutions in a subclass of generalized Proca theories with new internal symmetries [61,62].

In Refs. [59,60], analytic and numerical BH solutions have been systematically constructed for a wide class of generalized Proca theories. The power-law coupling models, which include the case of vector Galileons, can give rise to a variety of hairy BH solutions. The cubic and quartic couplings provide BH solutions with a primary Proca hair, whereas the sixth-order and intrinsic vector-mode couplings lead to BH solutions with a secondary Proca hair. On the other hand, there are no regular BHs for quintic power-law couplings due to the divergence of the longitudinal mode at a finite radius.

While both BHs and stars are compact objects with strong gravitational forces, their internal structures are different. For static and spherically symmetric BHs the metric and curvature generally exhibit the divergence at the center of spherical symmetry, but this is not the case for stars. Moreover, the configuration of stars is affected by different choices of the EOS through the change of the matter pressure. In this paper, we will study how the presence of derivative couplings in generalized Proca theories affects the mass and radius of relativistic stars. In Ref. [57], the authors studied NS solutions in a subclass of generalized Proca theories with the Lagrangian $\beta_4 G^{\mu\nu} A_\mu A_\nu$. We extend the analysis to more general cubic and quartic power-law derivative couplings and elucidate general properties of their effects on the mass and radius of relativistic stars.

For our purpose of investigating the effects of cubic and quartic derivative couplings on the mass and radius of relativistic stars in comparison with GR, we will restrict our numerical analysis to the case of the simplest polytropic EOS with two constant parameters [64]. We derive analytic solutions deep inside the star by imposing regular boundary conditions at the origin. The validity of analytic solutions will be confirmed by numerical integrations across the surface of the star for the polytropic EOS. We will also study the effects of sixth-order and intrinsic vector-mode couplings on the configuration of relativistic stars. However, we will not consider quintic derivative couplings because of the absence of regular BHs [59,60] as well as pathological behavior in the regime of weak gravity [50]. The essential qualitative features of relativistic stars in generalized Proca theories are not sensitive to the choice of EOSs.

We organize our paper as follows. In Sec. II, we derive a set of equations in generalized Proca theories with matter on the static and spherically symmetric background, and briefly review relativistic stars in GR and the polytrope EOS. In Secs. III and IV, we study how the mass and radius are modified by the presence of cubic and quartic power-law couplings, respectively. In Sec. V, we show that sixth-order and intrinsic vector-mode couplings lead to the relativistic star solutions identical to those in GR with a trivial vector field. We conclude in Sec. VI.

We work in centimeter-gram-second (CGS) units, where the speed of light, the reduced Planck constant, the gravitational constant, and the neutron mass are given by $c = 2.9989 \times 10^{10}\,\mathrm{cm\cdot s^{-1}}$, $\hbar = 1.0546 \times 10^{-27}\,\mathrm{erg\cdot s}$, $G = 6.6741 \times 10^{-8}\,\mathrm{g^{-1}\cdot cm^3\cdot s^{-2}}$, and $m_\mathrm{n} = 1.6749 \times 10^{-24}\,\mathrm{g}$, respectively.

II. GENERALIZED PROCA THEORIES AND RELATIVISTIC STARS

A. Equations of motion on the static and spherically symmetric background

The action of generalized Proca theories with a vector field A_μ is given by [39,42]

$$S=\int d^4x\sqrt{-g}\left[F+\sum_{i=2}^{6}\mathcal{L}_i+\mathcal{L}_m\right], \tag{2.1}$$

where g is a determinant of the metric tensor $g_{\mu\nu}$, $\mathcal{L}_m$ is a matter Lagrangian, and

$$\mathcal{L}_2=G_2(X,F,Y), \tag{2.2}$$

$$\mathcal{L}_3=G_3(X)\nabla_\mu A^\mu, \tag{2.3}$$

$$\mathcal{L}_4=G_4(X)R+G_{4,X}(X)[(\nabla_\mu A^\mu)^2-\nabla_\mu A_\nu\nabla^\nu A^\mu], \tag{2.4}$$

$$\begin{aligned}\mathcal{L}_5=&G_5(X)G_{\mu\nu}\nabla^\mu A^\nu-\frac{1}{6}G_{5,X}(X)[(\nabla_\mu A^\mu)^3\\&-3\nabla_\mu A^\mu\nabla_\rho A_\sigma\nabla^\sigma A^\rho+2\nabla_\rho A_\sigma\nabla^\nu A^\rho\nabla^\sigma A_\nu]\\&-g_5(X)\tilde{F}^{\alpha\mu}\tilde{F}^{\beta}{}_{\mu}\nabla_\alpha A_\beta,\end{aligned} \tag{2.5}$$

$$\mathcal{L}_6=G_6(X)L^{\mu\nu\alpha\beta}\nabla_\mu A_\nu\nabla_\alpha A_\beta+\frac{1}{2}G_{6,X}(X)\tilde{F}^{\alpha\beta}\tilde{F}^{\mu\nu}\nabla_\alpha A_\mu\nabla_\beta A_\nu, \tag{2.6}$$

with

$$\begin{aligned}&F_{\mu\nu}=\nabla_\mu A_\nu-\nabla_\nu A_\mu, \qquad F=-\frac{1}{4}F_{\mu\nu}F^{\mu\nu},\\&X=-\frac{1}{2}A_\mu A^\mu, \qquad Y=A^\mu A^\nu F_\mu{}^\alpha F_{\nu\alpha}.\end{aligned} \tag{2.7}$$

Here, ∇_μ, R, and $G_{\mu\nu}$ represent the covariant derivative, the Ricci scalar, and the Einstein tensor associated with the four-dimensional metric $g_{\mu\nu}$, respectively. While the function G_2 is generally dependent on X, F, Y, the functions $G_{3,4,5,6}$ and g_5 depend on X alone with the notation of partial derivatives $G_{i,X}\equiv\partial G_i/\partial X$. The dual strength tensor $\tilde{F}^{\mu\nu}$ and the double dual Riemann tensor $L^{\mu\nu\alpha\beta}$ are defined, respectively, by

$$\tilde{F}^{\mu\nu}=\frac{1}{2}\mathcal{E}^{\mu\nu\alpha\beta}F_{\alpha\beta}, \qquad L^{\mu\nu\alpha\beta}=\frac{1}{4}\mathcal{E}^{\mu\nu\rho\sigma}\mathcal{E}^{\alpha\beta\gamma\delta}R_{\rho\sigma\gamma\delta}, \tag{2.8}$$

where $\mathcal{E}^{\mu\nu\alpha\beta}$ is the Levi-Civita tensor satisfying the normalization $\mathcal{E}^{\mu\nu\alpha\beta}\mathcal{E}_{\mu\nu\alpha\beta}=-4!$, and $R_{\rho\sigma\gamma\delta}$ is the Riemann tensor. The Lagrangians containing the functions $g_5(X)$ and $G_6(X)$ correspond to intrinsic vector modes.

We consider a static and spherically symmetric background characterized by the line element

$$ds^2=-f(r)c^2dt^2+h^{-1}(r)dr^2+r^2(d\theta^2+\sin^2\theta d\varphi^2), \tag{2.9}$$

where f and h are functions of the distance r from the center of symmetry. On this background, the vector field can be expressed in the form

$$A_\mu=(cA_0(r),A_1(r),0,0), \tag{2.10}$$

where $A_1(r)$ is the r-derivative of a longitudinal scalar χ, such that $A_1(r)=d\chi/dr\equiv\chi'(r)$. The transverse mode $A_i^{(T)}$ in the spatial components A_i needs to vanish due to the regularity at the origin [49]. On the static and spherically symmetric background (2.9) with the vector components (2.10) there is the relation $Y=4FX$, so the additional dependence of Y in Eq. (2.2) can be removed [60].

We assume that the matter sector is described by a perfect fluid minimally coupled to gravity. Defining the matter energy-momentum tensor

$$T^{\mu\nu}\equiv\frac{2}{\sqrt{-g}}\frac{\delta(\sqrt{-g}\mathcal{L}_m)}{\delta g_{\mu\nu}}, \tag{2.11}$$

the mixed tensor T^μ_ν is expressed in the form

$$T^\mu_\nu=\mathrm{diag}(-\rho c^2,P,P,P), \tag{2.12}$$

where ρ is the total mass density and P is the pressure.

Varying the action (2.1) with respect to f,h,A_0,A_1, respectively, we obtain

$$\left(c_1+\frac{c_2}{r}+\frac{c_3}{r^2}\right)h'+c_4+\frac{c_5}{r}+\frac{c_6}{r^2}=\frac{\rho}{c^2}, \tag{2.13}$$

$$-\frac{h}{f}\left(c_1+\frac{c_2}{r}+\frac{c_3}{r^2}\right)f'+c_7+\frac{c_8}{r}+\frac{c_9}{r^2}=\frac{P}{c^4}, \tag{2.14}$$

where $c_{1,2,\ldots,9}$ are given in the Appendix, and

$$
\begin{aligned}
&rf[2fh(rA_0''+2A_0')+r(fh'-f'h)A_0'](1+G_{2,F})+r^2hA_0'^2[2fhA_0''-(f'h-fh')A_0']G_{2,FF}-2r^2f^2A_0G_{2,X}\\
&\quad-2r^2fA_0'(fh^2A_1A_1'-hA_0A_0'+f'hX_0-fh'X_1)G_{2,XF}-rfA_0[2rfhA_1'+(rf'h+rfh'+4fh)A_1]G_{3,X}\\
&\quad+4f^2A_0(rh'+h-1)G_{4,X}-8fA_0[rfh^2A_1A_1'-(rf'h+rfh'+fh)X_1]G_{4,XX}\\
&\quad-fA_0[f(3h-1)h'A_1+h(h-1)(f'A_1+2fA_1')]G_{5,X}-2fhA_0X_1[2fhA_1'+(f'h+fh')A_1]G_{5,XX}\\
&\quad-2f[f(3h-1)h'A_0'+h(h-1)(2fA_0''-f'A_0')]G_6-4fhA_0'X_1(hA_0A_0'-2fh^2A_1A_1'-2f'hX_0+2fh'X_1)G_{6,XX}\\
&\quad-2f[4fh^2X_1A_0''-2h(hX-X_0)f'A_0'+2f(6h-1)h'X_1A_0'+h(h-1)A_0A_0'^2-2fh^2(3h-1)A_0'A_1A_1']G_{6,X}\\
&\quad-4fh[2rfhA_1A_0''-\{(rf'h-3rfh'-2fh)A_1-2rfhA_1'\}A_0']g_5\\
&\quad-4rfhA_0'[hA_0A_0'A_1+4fhX_1A_1'-2A_1(f'hX_0-fh'X_1)]g_{5,X}=0,
\end{aligned}
\tag{2.15}
$$

$$
\begin{aligned}
&A_1[r^2fG_{2,X}-2(rf'h+fh-f)G_{4,X}+4h(rA_0A_0'-rf'X-fX_1)G_{4,XX}-hA_0'^2(3h-1)G_{6,X}-2h^2X_1A_0'^2G_{6,XX}]\\
&\quad=r[r(f'X-A_0A_0')+4fX_1]G_{3,X}+2f'hX_1G_{5,X}+(A_0A_0'-f'X)[(1-h)G_{5,X}-2hX_1G_{5,XX}]-2rhA_0'^2(g_5+2X_1g_{5,X}).
\end{aligned}
\tag{2.16}
$$

The quantity X is given by $X=X_0+X_1$, where

$$X_0\equiv\frac{A_0^2}{2f},\qquad X_1\equiv-\frac{hA_1^2}{2}. \tag{2.17}$$

From the matter continuity equation, it follows that

$$P'+\frac{f'}{2f}(\rho c^2+P)=0. \tag{2.18}$$

For a given EOS

$$P=P(\rho), \tag{2.19}$$

Eqs. (2.13)–(2.16) with Eq. (2.18) form a closed set of equations to determine f, h, A_0, A_1, ρ, and P as functions of r.

B. Relativistic stars in GR

Here, we briefly review relativistic stars in GR without the vector field A_μ. This corresponds to the functions

$$G_4=\frac{1}{16\pi G},\quad G_2=G_3=G_5=G_6=0,\quad g_5=0. \tag{2.20}$$

In this case, Eqs. (2.13) and (2.14) reduce, respectively, to

$$\frac{h'}{r}+\frac{h-1}{r^2}=-\frac{8\pi G\rho}{c^2}, \tag{2.21}$$

$$\frac{hf'}{f\,r}+\frac{h-1}{r^2}=\frac{8\pi GP}{c^4}. \tag{2.22}$$

Introducing the mass function $M(r)$, as

$$h(r)=1-\frac{2GM(r)}{c^2r}, \tag{2.23}$$

we can express Eq. (2.21) in the simple form

$$M'(r)=4\pi\rho r^2. \tag{2.24}$$

On using Eqs. (2.22) and (2.23), the continuity equation (2.18) reduces to the Tolman-Oppenheimer-Volkoff (TOV) equation

$$P'(r)=-\frac{G(\rho+P/c^2)(M+4\pi r^3P/c^2)}{r^2[1-2GM/(c^2r)]}. \tag{2.25}$$

Around the center of the star, we expand f, h, ρ, and P in the following forms:

$$
\begin{aligned}
&f(r)=1+\sum_{i=2}^{\infty}f_ir^i,\qquad h(r)=1+\sum_{i=2}^{\infty}h_ir^i,\\
&\rho(r)=\rho_c+\sum_{i=2}^{\infty}\rho_ir^i,\qquad P(r)=p_c+\sum_{i=2}^{\infty}p_ir^i,
\end{aligned}
\tag{2.26}
$$

where f_i, h_i, ρ_i, p_i are constants. Then, the regularity conditions $f'(0)=h'(0)=\rho'(0)=P'(0)=0$ are satisfied with $\rho(r)$ and $P(r)$ converging to constant values ρ_c and p_c, respectively, as $r\to0$. By solving Eqs. (2.21), (2.22), and (2.18) iteratively, the boundary conditions around $r=0$ can be found as

$$f(r)=1+\frac{4\pi G(c^2\rho_c+3p_c)}{3c^4}r^2+\mathcal{O}(r^4), \tag{2.27}$$

$$h(r)=1-\frac{8\pi G\rho_c}{3c^2}r^2+\mathcal{O}(r^4), \tag{2.28}$$

$$P(r) = p_c - \frac{2\pi G(c^2\rho_c + 3p_c)(c^2\rho_c + p_c)}{3c^4} r^2 + \mathcal{O}(r^4). \tag{2.29}$$

The numerical integration is performed until reaching the surface of the star $r = R_*$, where $P(R_*) = 0$. By requiring the continuity of metric functions and their first-order derivatives across the surface $r = R_*$, the internal solution is smoothly joined to the exterior Schwarzschild solution given by the metric (2.9) with

$$f = h = 1 - \frac{2GM_*}{c^2 r}, \tag{2.30}$$

where the Arnowitt-Deser-Misner (ADM) mass is given by $M_* \equiv M(R_*)$. Provided that the EOS (2.19) inside the star is known, it is practically more convenient to integrate Eqs. (2.22), (2.24), and (2.25) to determine $\rho(r)$, $P(r)$, and $M(r)$. In Secs. III–V, the mass and radius of relativistic stars in generalized Proca theories will be compared to those in GR.

C. The polytrope equation of state

As we will see later, the qualitative results of relativistic stars in generalized Proca theories do not depend on the choice of EOSs. Thus, in this paper, we focus on one of the simplest EOSs, known as the polytropic EOS, which is given by

$$P = \mathcal{K}\rho_0^\Gamma, \tag{2.31}$$

where ρ_0 is the rest-mass density, and $\mathcal{K}$, Γ are constants. In general, the total energy density ρc^2 is expressed in the form $\rho c^2 = \rho_0 c^2(1+\epsilon)$, where ϵ is the dimensionless internal energy density per unit mass. For baryons with number density n_b and the mean rest mass m_b, the rest-mass density is given by $\rho_0 = n_b m_b$. On using the first law of thermodynamics for the adiabatic process, the baryon pressure is expressed as $P = n_b^2 m_b c^2 \partial\epsilon/\partial n_b$ [64]. For the polytropic EOS (2.31), i.e., $P = \mathcal{K}(n_b m_b)^\Gamma$, we obtain the integrated solution $\epsilon = \mathcal{K}\rho_0^{\Gamma-1}/[c^2(\Gamma-1)]$, so the total mass density yields $\rho = \rho_0 + \mathcal{K}\rho_0^\Gamma/[c^2(\Gamma-1)]$. We define the dimensionless rest-mass density χ and the rescaled polytropic gas constant K as

$$\chi \equiv \frac{\rho_0}{\tilde{\rho}_0} = \frac{n_b}{n_0}, \qquad K \equiv \frac{\mathcal{K}}{\tilde{\rho}_0^{1-\Gamma}c^2}, \tag{2.32}$$

with

$$\tilde{\rho}_0 = n_0 m_b, \tag{2.33}$$

where $n_0 = 0.1\ (\mathrm{fm})^{-3}$ is the typical nuclear number density of relativistic stars. As a result, the polytropic EOS can be expressed in the form [13]

$$\rho = \tilde{\rho}_0\left(\chi + \frac{K}{\Gamma-1}\chi^\Gamma\right), \qquad P = K\tilde{\rho}_0 c^2 \chi^\Gamma, \tag{2.34}$$

with

$$w \equiv \frac{P}{\rho c^2} = \frac{K\chi^{\Gamma-1}}{1 + K\chi^{\Gamma-1}/(\Gamma-1)}. \tag{2.35}$$

In the nonrelativistic regime characterized by $K\chi^{\Gamma-1} \ll 1$, we have $w \simeq K\chi^{\Gamma-1}$, so w grows with the increase of mass density ρ. In the relativistic regime, w approaches a constant value $\Gamma - 1$ for increasing ρ.

For numerical purposes, it is convenient to introduce the dimensionless quantities:

$$x = \frac{r}{r_0}, \quad y = \frac{\rho}{\tilde{\rho}_0}, \quad w_0 = \frac{P}{\tilde{\rho}_0 c^2}, \quad m(r) = \frac{3M(r)}{4\pi\tilde{\rho}_0 r_0^3}, \tag{2.36}$$

where

$$r_0 = \sqrt{\frac{c^2}{G\tilde{\rho}_0}}. \tag{2.37}$$

In the following, we identify m_b with the neutron mass $m_\mathrm{n} = 1.6749 \times 10^{-24}$ g. Then, the distance (2.37) corresponds to $r_0 = 89.696$ km, with $\tilde{\rho}_0 = 1.6749 \times 10^{14}\ \mathrm{g\,cm^{-3}}$. The polytropic EOS (2.34) can be expressed in the form

$$w_0(x) = K\chi(x)^\Gamma, \quad y(x) = \left(\frac{w_0(x)}{K}\right)^{1/\Gamma} + \frac{w_0(x)}{\Gamma-1}. \tag{2.38}$$

Specifying the value of $w_0(0)$, the associated dimensionless density $y_c = \rho_c/\tilde{\rho}_0$ is also fixed at the center of the star. The star radius R_* is defined by

$$w_0(x_*) = 0, \tag{2.39}$$

where $x_* = R_*/r_0$. By choosing different boundary conditions of w_0 at $x = 0$, we obtain the configuration of relativistic stars with different mass M_* and radius R_*. In terms of the solar mass $M_\odot = 1.9884 \times 10^{33}$ g, we can express the ADM mass M_* in the form

$$M_* = 2.5462 \times 10^2 m(x_*) M_\odot. \tag{2.40}$$

For comparison with observational data of NSs, however, we would need phenomenologically parametrized EOSs specifying the stiffness of the star in several density intervals [65]. In this paper, we will not perform the comparison with observational data of NSs, but we focus

on how vector-field derivative couplings modify the mass-radius relation of relativistic stars from GR by considering the polytropic EOS (2.34) with two constant parameters Γ and K. As we will see below, the qualitative behavior of vector-field derivative couplings on the mass and radius of relativistic stars, which can be analytically understood to some degree, is generally insensitive to the choice of EOSs. For numerics, we choose the index $\Gamma = 2.34$ in Secs. III and IV.

III. CUBIC COUPLINGS

Let us begin with the cubic derivative interaction $G_3(X)$. For concreteness, we study the power-law coupling given by

$$G_3 = \beta_3 X^n, \tag{3.1}$$

where β_3 is a constant and n is a positive integer. We also take into account the Einstein-Hilbert term $G_4 = 1/(16\pi G)$ in the action (2.1), with $G_2 = G_5 = G_6 = 0$ and $g_5 = 0$. We consider the models with positive integer n, which includes the vector Galileon as a special case ($n = 1$). From Eq. (2.16), the longitudinal component is related to A_0, f, h and their derivatives as

$$A_1 = \epsilon\sqrt{\frac{rA_0(f'A_0 - 2fA_0')}{fh(rf' + 4f)}}, \tag{3.2}$$

where $\epsilon = \pm 1$.

A. Analytic solutions around the center of the star

We first derive analytic solutions to the metrics, the vector field, and the pressure around $r = 0$. We take the positive branch of Eq. (3.2) and differentiate it with respect to r. Then, A_1 and A_1' are substituted into Eqs. (2.13)–(2.15) to eliminate the dependence of the longitudinal mode.

Around the center of the star, we expand f, h, ρ, P in the forms (2.26). The temporal vector component is also expanded as

$$A_0 = a_0 + \sum_{i=2}^{\infty} a_i r^i, \tag{3.3}$$

where a_0 and a_i are constants. These solutions satisfy the regular boundary conditions $f'(0) = h'(0) = \rho'(0) = P'(0) = 0$ and $A_0'(0) = 0$. Without loss of generality, we will assume that $a_0 > 0$. We also require the condition $P''(0) < 0$ for the pressure [66]. Expanding the continuity equation (2.18) around the origin, we obtain

$$p_2 = -\frac{\rho_c c^2 + p_c}{2} f_2. \tag{3.4}$$

The condition $P''(0) < 0$, which corresponds to $p_2 < 0$, is satisfied for

$$f_2 > 0. \tag{3.5}$$

From Eq. (3.2), the leading-order solution of the longitudinal mode around the center of the star is given by

$$A_1 = \sqrt{\frac{a_0(a_0 f_2 - 2a_2)}{2}} r, \tag{3.6}$$

which ensures the regularity of A_1 at $r = 0$. For the existence of this solution, we require that

$$a_0(a_0 f_2 - 2a_2) > 0. \tag{3.7}$$

Substituting Eq. (3.3) into Eqs. (2.13)–(2.15) and solving them iteratively, we obtain the following solutions around the origin:

$$f(r) = 1 + \frac{4\pi}{3}(1 + 3w_c + \mathcal{F})\frac{r^2}{r_c^2} + \mathcal{O}(r^4), \tag{3.8}$$

$$h(r) = 1 - \frac{8\pi}{3}(1 + \mathcal{F})\frac{r^2}{r_c^2} + \mathcal{O}(r^4), \tag{3.9}$$

$$A_0(r) = \frac{\bar{a}_0}{\sqrt{8\pi G}}\left(1 + \frac{4\pi}{3}\frac{\mathcal{F}}{\bar{a}_0^2}\frac{r^2}{r_c^2}\right) + \mathcal{O}(r^4), \tag{3.10}$$

$$P(r) = p_c - \frac{2\pi}{3}(\rho_c c^2 + p_c)(1 + 3w_c + \mathcal{F})\frac{r^2}{r_c^2} + \mathcal{O}(r^4), \tag{3.11}$$

where

$$\mathcal{F} \equiv \frac{3n^2 \bar{a}_0^{2n+1}\bar{\beta}_3}{2^{2n+3}\pi}\left[-\bar{\beta}_3 \bar{a}_0^{2n-1}\left(1 - \frac{\bar{a}_0^2}{2}\right) \pm \sqrt{\bar{\beta}_3^2 \bar{a}_0^{4n-2}\left(1 - \frac{\bar{a}_0^2}{2}\right)^2 + \frac{2^{2n+3}\pi}{3n^2}(1 + 3w_c)}\right], \tag{3.12}$$

with the dimensionless constants defined by

$$\bar{\beta}_3 \equiv \frac{\beta_3 r_c}{(\sqrt{8\pi G})^{2n-1}}, \qquad \bar{a}_0 \equiv \sqrt{8\pi G}\, a_0,$$
$$r_c \equiv \sqrt{\frac{c^2}{G\rho_c}}, \qquad w_c \equiv \frac{p_c}{\rho_c c^2}. \tag{3.13}$$

In the limit that $\beta_3 \to 0$, the iterative solutions (3.8), (3.9), and (3.11) recover the general relativistic solutions (2.27)–(2.29). The density $\rho(r)$ is known for a given EOS. Using Eq. (3.8) with Eq. (3.12), the condition (3.5) translates to

$$|\bar{\beta}_3|\bar{a}_0^{2n} < \frac{2^{n+1}}{n}\sqrt{\frac{\pi(1+3w_c)}{3}}. \tag{3.14}$$

Under this bound, the condition (3.7) is automatically satisfied. The EOS w_c is bounded from above with the maximum value of order 1. For the polytropic EOS (2.35), we have that $w_c < \Gamma - 1$. Then, $|\bar{\beta}_3|\bar{a}_0^{2n} \lesssim 2^{n+1}/n$ from Eq. (3.14). For $n = \mathcal{O}(1)$, the product $|\bar{\beta}_3|\bar{a}_0^{2n}$ is constrained to be smaller than order 1. For the branch of the positive sign in Eq. (3.12), the upper bound (3.14) corresponds to the negative value of $\bar{\beta}_3$, whereas, for the negative sign, the upper limit of $\bar{\beta}_3$ is positive. In the following, we will focus on the case of the positive sign in Eq. (3.12) without loss of generality. Then, for $\bar{\beta}_3 < 0$, the term $\mathcal{F}$ in Eq. (3.11) is negative, so the negative coupling $\bar{\beta}_3$ effectively increases the pressure. In other words, the positive term $1 + 3w_c$ in Eq. (3.11) is partially compensated by the negative term $\mathcal{F}$. This means that, with increasing r, the pressure $P(r)$ decreases more slowly relative to the case $\bar{\beta}_3 = 0$ at least around the center of the body. Then, we expect that the negative coupling $\bar{\beta}_3$ may lead to a larger radius of the star than that for $\bar{\beta}_3 = 0$.

Indeed, the negative value of $\bar{\beta}_3$ close to the upper bound of Eq. (3.14) gives rise to the pressure (3.11) which is nearly constant around the center of the star. Then, we may anticipate that the radius of the star can be infinitely large. However, we will show that this is not the case. From

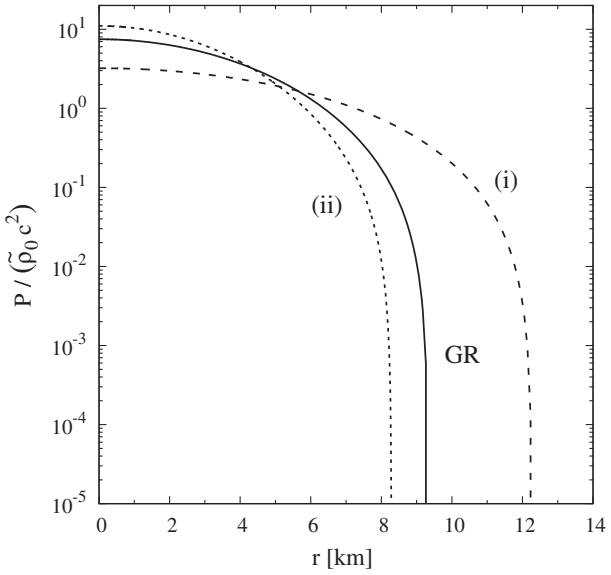

FIG. 1. Variation of the pressure in cubic Galileons ($G_3 = \beta_3 X$) for the polytropic EOS (2.34) with $K = 0.0130$ and $\Gamma = 2.34$. The two cases (i) and (ii) correspond to (i) $\tilde{\beta}_3 = -1$, $\bar{a}_0 = 2.2$, $\chi(r) = 10.471$ at $r/r_0 = 10^{-3}$ and (ii) $\tilde{\beta}_3 = 1$, $\bar{a}_0 = 2.0$, $\chi(r) = 17.783$ at $r/r_0 = 10^{-3}$, respectively. We also show the case of GR with $\tilde{\beta}_3 = 0$, $\bar{a}_0 = 0$, $\chi(r) = 15.136$ at $r/r_0 = 10^{-3}$. The boundary conditions of f, h, A_0, P are chosen to be consistent with Eqs. (3.8)–(3.11).

Eqs. (2.23) and (3.9) the mass function around $r = 0$ is given by

$$M(r) = \frac{4}{3}\pi\rho_c r^3(1+\mathcal{F}) + \mathcal{O}(r^5). \tag{3.15}$$

The negative coupling $\bar{\beta}_3$ leads to the decrease of $M(r)$ relative to the case of GR. For the theoretical consistency, we require that $M(r) > 0$ around the center of body. This amounts to the condition $\mathcal{F} > -1$, which translates to

$$|\bar{\beta}_3|\bar{a}_0^{2n} < \frac{2^{n+1}}{n}\sqrt{\frac{2\pi}{3(2+3w_c\bar{a}_0^2)}}, \tag{3.16}$$

which is tighter than the bound (3.14). Substituting $\mathcal{F} = -1$ into Eq. (3.11), the pressure corresponding to the maximum value of $|\bar{\beta}_3|$ in Eq. (3.16) is given by

$$P_{\max}(r) = p_c\left[1 - 2\pi(1+w_c)\frac{r^2}{r_c^2}\right], \tag{3.17}$$

which decreases for increasing r. This expression is valid around $r = 0$, but we extrapolate it to the surface of the star to provide a crude criterion for the upper limit of the radius R_*. Then, we obtain the bound

$$R_* \lesssim \frac{r_c}{\sqrt{2\pi(1+w_c)}}, \tag{3.18}$$

which means that R_* is constrained to be smaller than the order of r_c. Since the rhs of Eq. (3.18) does not depend on the power n, the maximum radius is insensitive to the form of cubic couplings $G_3(X)$.

To discuss the dynamical stability of relativistic stars, we define the proper mass

$$M_p \equiv \int_{R\le R_*} d^3x\rho\sqrt{{}^{(3)}g} = \int_0^{R_*}\frac{4\pi\rho r^2}{\sqrt{h}}dr, \tag{3.19}$$

where ${}^{(3)}g$ is the determinant of a three-dimensional spatial metric. The gravitational binding energy is defined by the difference between M_p and the ADM mass M_*, i.e.,

$$\Delta \equiv (M_p - M_*)c^2. \tag{3.20}$$

The star with $\Delta > 0$ is gravitationally bound and the condition $\Delta > 0$ can be regarded as a necessary condition for its dynamical stability, whereas the star with $\Delta < 0$ is not bound and hence dynamically unstable. For $\bar{\beta}_3 < 0$ the r-derivative of the leading-order term on the rhs of Eq. (3.15) is smaller than $4\pi\rho_c r^2$, whereas the term inside the integral of Eq. (3.19) is larger than $4\pi\rho r^2$. This implies that the condition $\Delta > 0$ may hold for $\bar{\beta}_3 < 0$, but we need

to caution for readers that Eq. (3.15) is valid only around the central region of the star.

B. Numerical solutions

The above analytic solutions have been derived under the expansion around $r = 0$. In order to study the effect of the coupling β_3 on the mass M_* and the radius R_* of relativistic stars more precisely, we numerically solve Eqs. (2.13)–(2.16) with Eq. (2.18) for the polytropic EOS (2.34) by using the boundary conditions (3.8)–(3.11) around the origin. For numerical computations, we will focus on the case of vector Galileons, i.e., $n = 1$ in Eq. (3.1). The numerical integration is performed until reaching the surface $r = R_*$ characterized by the condition $w_0(R_*) = 0$, where w_0 is defined in Eq. (2.36). By requiring the continuity of metric functions, the vector field, and their first-order derivatives across the surface $r = R_*$ and using their values at $r = R_*$ as boundary conditions, the exterior solution can be obtained by integrating Eqs. (2.13)–(2.16) in the vacuum region $r > R_*$, where $\rho = P = 0$. The consistent exterior solutions of the star approach the iterative solutions in the large r limit characterized by three parameters including the ADM mass M_* [see Eqs. (5.10)–(5.13) of Ref. [60]].

In Fig. 1, we plot the normalized pressure $P/(\tilde{\rho}_0 c^2)$ versus the distance r from the center of the star with $K = 0.013$ and $\Gamma = 2.34$ for three different values of $\tilde{\beta}_3 \equiv \beta_3 r_0/\sqrt{8\pi G} = \bar{\beta}_3 r_0/r_c$. In GR, the pressure varies according to Eq. (2.29) at small distances. As we observe in Fig. 1, $P(r)$ starts to decrease rapidly around the surface of the star. In the numerical simulation of Fig. 1, the star radius is $R_* \simeq 9.3$ km for $\beta_3 = 0$. In the presence of negative coupling β_3, the pressure decreases more slowly with increasing r; see case (i) of Fig. 1. In case (i), we have chosen a smaller value of the central pressure relative to that in GR, but the smaller decreasing rate of $P(r)$ in the former leads to the larger radius, $R_* \simeq 12.3$ km. The case (ii) in Fig. 1 corresponds to a positive value of β_3, with a larger central pressure compared to the GR case. The decreasing rate of $P(r)$ in case (ii) is faster than that in GR, so the resulting radius is smaller, $R_* \simeq 8.3$ km.

Similarly, the density $\rho(r)$ also decreases as a function of r. The central density ρ_c in case (i) is smaller than that in GR, while the radius R_* is larger. Since the density $\rho(r)$ in case (i) decreases more slowly relative to the case of GR, the former catches up with the latter at an intermediate distance ($r \simeq 6$ km). The r-derivative of the mass function $M(r)$ can be generally written in the form

$$M'(r) = 4\pi\rho(r)r^2[1 + \tilde{\mathcal{F}}(r)], \tag{3.21}$$

where $\tilde{\mathcal{F}}(r)$ is a function of r containing the dependence of β_3. As we estimated in Eq. (3.15), the functions $\rho(r)$ and $\tilde{\mathcal{F}}(r)$ around $r = 0$ reduce to the constants ρ_c and $\mathcal{F}$, respectively. When we integrate Eq. (3.21) with respect to r, the first term on the rhs gives rise to a contribution to M_* which is roughly proportional to $(4\pi/3)\rho_c R_*^3$. The increase of R_* induced by the negative coupling β_3 leads to a larger contribution to M_* relative to the decrease of ρ_c. In case (i) the mass contribution arising from the integration of the term $4\pi\rho(r)r^2$ in Eq. (3.21) is $M_{*1} = 2.87\ M_\odot$, which is larger than the value $M_{*1} = 1.67\ M_\odot$ of GR in Fig. 1. The ratio of R_*^3 between the case (i) and GR is given by $(12.3/9.3)^3 = 2.31$. This increase is slightly compensated by the smaller density in the central region with the decrease at about 25%, so the resulting ratio of M_{*1} between the two cases becomes $2.87/1.67 = 1.72 < 2.31$.

For $\beta_3 < 0$ the function $\tilde{\mathcal{F}}(r)$ in Eq. (3.21) is negative around $r = 0$, so the negative coupling works to reduce the mass term M_{*1}. In case (i) of Fig. 1, the mass M_{*2} arising from the numerical integration of $4\pi\rho(r)r^2\tilde{\mathcal{F}}(r)$ is found to be $M_{*2} \simeq -0.29M_{*1}$, so the total mass $M_* = M_{*1} + M_{*2}$ can be estimated as $M_* \simeq 0.71M_{*1} \simeq 2.03\ M_\odot$. The mass function $M(r)$ in case (i) is smaller than that in GR except for the distance r around the surface of the star. However, the increase of $M(r)$ in case (i) continuously occurs up to the radius R_* larger than that in GR, so the resulting mass M_* in the former is larger. Thus, the main reason for the increase of M_* comes from the increase of R_* induced by the negative coupling.

For $\beta_3 > 0$, the radius R_* gets smaller compared to the value in GR; see case (ii) of Fig. 1. Since the function $\tilde{\mathcal{F}}(r)$ in Eq. (3.21) is positive, the mass function $M(r)$ is larger than that in GR at small distances. However, the increase of $M(r)$ stops at a smaller radius R_*, which results in a smaller mass M_*. Hence the positive coupling β_3 generally leads to the decrease of mass M_* relative to the GR case.

In Fig. 2, we plot the mass-radius relation for the polytropic EOS (2.34) with $K = 0.0130$ and $\Gamma = 2.34$. The central density is chosen to be in the range $y_c = \rho_c/\tilde{\rho}_0 \leq 200$. In this case, the maximum ADM mass M_* in GR is given by $M_{\rm max} = 1.67\ M_\odot$ with the radius $R_* = 9.3$ km and the central density $\rho_c = 3.5 \times 10^{15}\ {\rm g \cdot cm^{-3}}$ (plotted as the GR case in Fig. 1). For increasing negative coupling $|\beta_3|$, the maximum mass gets larger. This effect tends to be significant for $|\tilde{\beta}_3|\bar{a}_0^2$ exceeding the order of 1. The maximum mass reached for $\tilde{\beta}_3 = -1$ and $\bar{a}_0 = 2.2$ [case (c) in Fig. 2] is $M_{\rm max} = 2.03M_\odot$, with the radius $R_* = 12.3$ km and the central density $\rho_c = 2.1 \times 10^{15}\ {\rm g \cdot cm^{-3}}$ [plotted as case (i) of Fig. 1]. Even though ρ_c is smaller than that in GR, the larger radius R_* leads to the maximum mass $M_{\rm max}$ which is about $2.03/1.67 = 1.22$ times as large as that in GR.

From Eq. (3.16), there is the constraint $|\bar{\beta}_3|\bar{a}_0^2 < 4\sqrt{2\pi/[3(2 + 3w_c\bar{a}_0^2)]}$ for $n = 1$. If $\tilde{\beta}_3 = -1$, $w_c = 0.247$, $\rho_c/\rho_0 = 12.8$, this bound translates to $\bar{a}_0 < 2.7$. For increasing $\bar{a}_0$, the resulting mass of the star tends to be larger. In case (d) shown in Fig. 2 ($\tilde{\beta}_3 = -1$, $\bar{a}_0 = 2.4$), the

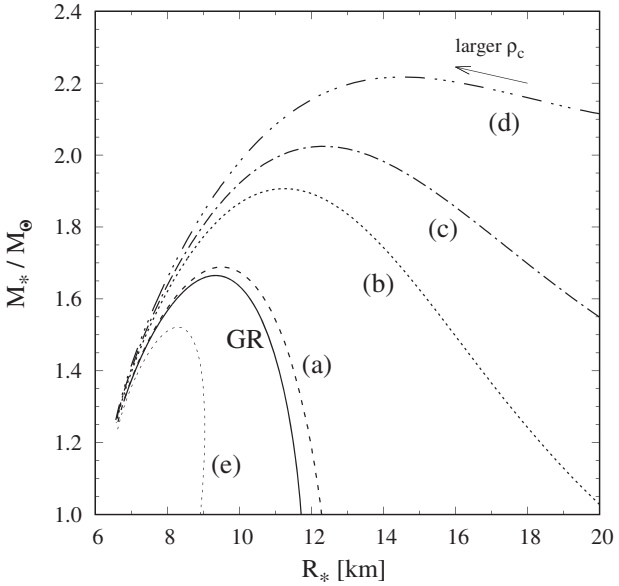

FIG. 2. Mass-radius relations in cubic Galileons for the polytropic EOS (2.34) with $\Gamma = 2.34$, $K = 0.0130$. We choose the boundary conditions (3.8)–(3.11) at the distance $r = 10^{-3} r_0$. Each curve corresponds to (a) $\tilde{\beta}_3 = -1$, $\bar{a}_0 = 1.0$, (b) $\tilde{\beta}_3 = -1$, $\bar{a}_0 = 2.0$, (c) $\tilde{\beta}_3 = -1$, $\bar{a}_0 = 2.2$, (d) $\tilde{\beta}_3 = -1$, $\bar{a}_0 = 2.4$, (e) $\tilde{\beta}_3 = +1$, $\bar{a}_0 = 2.0$, and the GR case $\tilde{\beta}_3 = 0$, $\bar{a}_0 = 0$. With increasing ρ_c, the values of M_* and R_* shift to the direction shown as the arrow inside the figure.

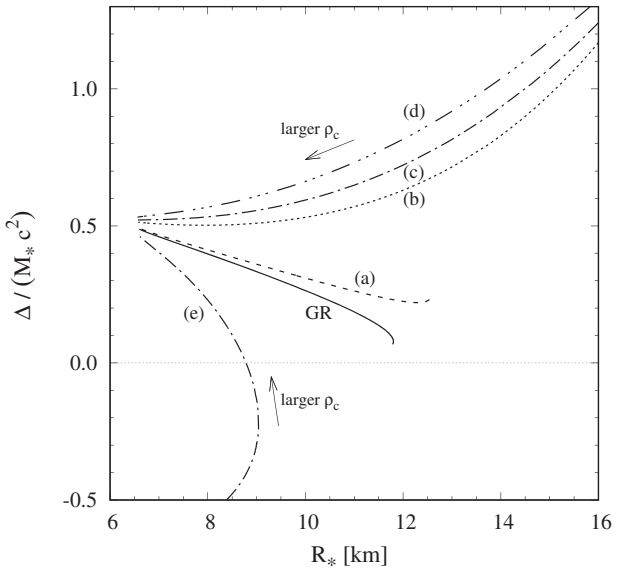

FIG. 3. The gravitational binding energy Δ normalized by $M_* c^2$ versus the radius R_* in cubic Galileons for the polytropic EOS (2.34), with $K = 0.0130$ and $\Gamma = 2.34$ in the region of the central density $3 \leq y_c \leq 200$. Each curve corresponds to the cases plotted in Fig. 2. With increasing ρ_c, the values of Δ and R_* shift to the direction shown as the arrow inside the figure.

maximum mass for the radius $R_* < 20$ km is given by $M_{\rm max} = 2.22\ M_\odot$. For $2.5 \lesssim \bar{a}_0 < 2.7$, M_* changes to a continuously growing function with respect to R_*. This property may be understood by using Eq. (3.11) for $|\tilde{\beta}_3| \bar{a}_0^2$ close to the upper bound (3.16). In this case, the star radius can be crudely estimated as

$$R_* \approx r_0 \sqrt{\frac{\rho_0}{2\pi(1+w_c)\rho_c}}. \tag{3.22}$$

In the regime $w_c \ll 1$, the radius has the dependence $R_* \propto \rho_c^{-1/2}$, so it increases for decreasing ρ_c. The quantity $\rho_c R_*^3$ also increases for smaller ρ_c, as $\rho_c R_*^3 \propto \rho_c^{-1/2} \propto R_*$. While the negative coupling $\tilde{\beta}_3$ suppresses the growth of $M(r)$ around $r = 0$, this is compensated by the increase of R_* in the region of small ρ_c. Hence, for $|\tilde{\beta}_3| \bar{a}_0^2$ close to the upper bound (3.16), the mass M_* continuously grows with the increase of R_*. Unless $\bar{a}_0$ is very close to the upper limit 2.7, the maximum mass $M_{\rm max}$ does not exceed $3\ M_\odot$ for $R_* < 20$ km with the model parameters used in Fig. 2.

If the quantity $|\tilde{\beta}_3| \bar{a}_0^2$ exceeds the upper limit set by Eq. (3.16), the mass function $M(r)$ is negative around the center of the star. Indeed, we numerically confirmed that the mass function enters the region $M(r) < 0$ around $r = 0$ and then $M(r)$ becomes positive at the distance away from the center. We regard that this situation is unphysical.

As we see in case (e) of Fig. 2, the positive coupling β_3 leads to smaller M_* and R_* than those in GR. In Fig. 3, we plot the quantity $\Delta/(M_* c^2) = M_p/M_* - 1$ versus the radius R_* for the same model parameters as those used in Fig. 2, where M_p is the proper mass defined by Eq. (3.19). For $\beta_3 < 0$, the binding energy Δ is always positive, so the star is gravitationally bound. For $\beta_3 > 0$, the star tends to be dynamically unstable in the region of small ρ_c. The configuration of maximum mass $M_* = 1.52\ M_\odot$ in case (e) of Fig. 2 ($\tilde{\beta}_3 = +1$ and $\bar{a}_0 = 2.0$), which corresponds to the central density $\rho_c = 4.3 \times 10^{15}\ {\rm g \cdot cm^{-3}}$ and the radius $R_* = 8.3$ km, leads to a positive binding energy, but the sign of Δ changes to negative for $\rho_c < 2.6 \times 10^{15}\ {\rm g \cdot cm^{-3}}$.

For the ranges of ρ_c smaller than those plotted as the cases (b)–(d) of Fig. 3, we numerically find that there is a maximum value of $\Delta/(M_* c^2)$ and then the binding energy gets smaller for decreasing ρ_c further. In the intermediate regime where $\Delta/(M_* c^2)$ decreases with the increase of ρ_c, there is the "repulsive" gravity effect induced by the negative coupling β_3. The pressure increased by the negative coupling β_3 can support the star with a stronger gravitational force. In other words, the increased binding energy in the intermediate regime of ρ_c is compatible with the large effective pressure induced by β_3.

The above discussion shows that the sign and the strength of coupling β_3 as well as the amplitude of A_0 play an important role for increasing the mass and radius of star. Around $r = 0$, the temporal component is given by Eq. (3.10), so the derivative $|A_0'|$ grows in proportion

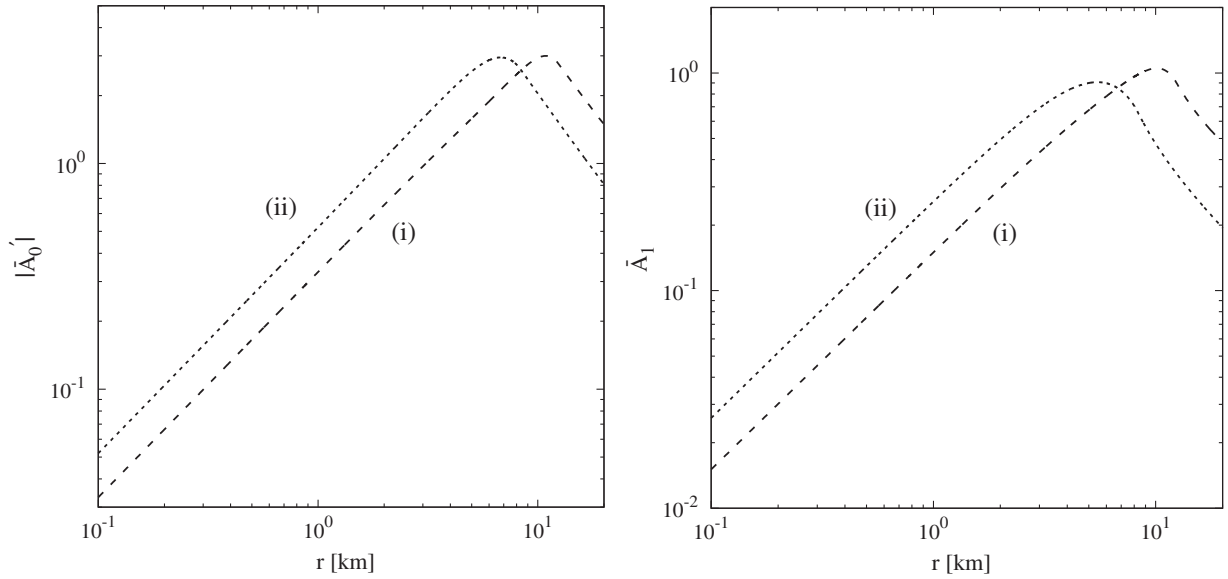

FIG. 4. Numerical solutions to the derivative $|\bar{A}_0'| = \sqrt{8\pi G} r_0 |A_0'|$ (left) and the longitudinal mode $\bar{A}_1 = \sqrt{8\pi G} A_1$ (right) in cubic Galileons for the polytropic (2.34) with $K = 0.0130$ and $\Gamma = 2.34$. The cases (i) and (ii) correspond to the same model parameters and boundary conditions as those used in Fig. 1.

to r. The longitudinal mode A_1 has the same r-dependence as $|A_0'|$ around $r = 0$; see Eq. (3.6). For increasing $|a_0|$, the amplitude of A_1 also tends to be larger. In Fig. 4, we plot $|A_0'|$ and A_1 versus r for the cases (i) and (ii) shown in Fig. 1. In both cases, $|A_0'|$ and A_1 increase in proportion to r up to the distance close to the surface of the star. Outside the body ($r > R_*$), the behavior of the vector field is similar to the vacuum solution around the static and spherically symmetric BHs derived in Refs. [59,60]. Namely, both $|A_0'|$ and A_1 decrease as $\propto 1/r^2$ for $r \gg R_*$. As in Refs. [59,60], the coupling β_3 induces some difference between the two metric components f and h around the surface of the star, but the difference becomes negligible in the limit that $r \gg R_*$.

IV. QUARTIC COUPLINGS

In this section, we study the effect of quartic derivative couplings $G_4(X)$ on the configuration of relativistic stars. We consider the power-law coupling model given by

$$G_4 = \frac{1}{16\pi G} + \beta_4 X^n, \tag{4.1}$$

with $G_2 = G_3 = G_5 = G_6 = 0$ and $g_5 = 0$, where β_4 is a constant and n is a positive integer. In Ref. [40], the authors discussed the relativistic star solutions for the specific case $n = 1$. Now, we investigate the models of general power n including the quartic vector Galileon ($n = 2$). From Eq. (2.16), the longitudinal mode obeys

$$\begin{aligned}&\beta_4 A_1 (A_0^2 - f h A_1^2)^{n-2} [A_1^2 f h \{(1 + h - 2nh) f \\ &\quad + (1 - 2n) r f' h\} + A_0^2 \{f(h-1) + (2n-1) r f' h\} \\ &\quad - 4r(n-1) A_0 A_0' f h] = 0.\end{aligned} \tag{4.2}$$

This gives rise to the two branches characterized by $A_1 = 0$ or $A_1 \neq 0$. For the latter branch, our numerical analysis shows that the solutions are qualitatively similar to those of cubic derivative couplings discussed in Sec. III. Hence we will focus on the other branch,

$$A_1 = 0, \tag{4.3}$$

in the rest of this section.

A. Analytic solutions around the center of star

Let us first derive analytic solutions to f, h, A_0, P by using the expansions (2.26) and (3.3) around $r = 0$. From the continuity equation (2.18), we obtain the same relation as in Eq. (3.4) among the coefficients p_2 and f_2. Substituting $A_1 = 0$ and $A_1' = 0$ into Eqs. (2.13)–(2.15), we obtain the iterative solutions

$$f(r) = 1 + f_2 r^2 + \mathcal{O}(r^4), \tag{4.4}$$

$$h(r) = 1 - \frac{8\pi}{3[1 - 2^{1-n}(2n-1)\bar{\beta}_4 \bar{a}_0^{2n}]} \frac{r^2}{r_c^2} + \mathcal{O}(r^4), \tag{4.5}$$

$$\begin{aligned}A_0(r) = &\frac{1}{\sqrt{8\pi G}} \left[\bar{a}_0 + \frac{2^{4-n} \pi n \bar{\beta}_4 \bar{a}_0^{2n-1}}{3\{1 - 2^{1-n}(2n-1)\bar{\beta}_4 \bar{a}_0^{2n}\}} \frac{r^2}{r_c^2}\right] \\ &+ \mathcal{O}(r^4),\end{aligned} \tag{4.6}$$

$$P(r) = p_c - \frac{c^2\rho_c + p_c}{2} f_2 r^2 + \mathcal{O}(r^4), \tag{4.7}$$

where the definitions of $\bar{a}_0, r_c, w_c$ are the same as those given in Eq. (3.13), and

$$\bar{\beta}_4 = \frac{\beta_4}{(8\pi G)^{n-1}}, \tag{4.8}$$

$$f_2 = \frac{4\pi[1 + 3w_c + 2^{1-n}\{1 - 3(2n-1)w_c\}\bar{\beta}_4\bar{a}_0^{2n} - 2^{5-2n}n^2\bar{\beta}_4^2\bar{a}_0^{4n-2}]}{3[1 - 2^{1-n}(2n-1)\bar{\beta}_4\bar{a}_0^{2n}]^2 r_c^2}. \tag{4.9}$$

Without loss of generality, we assume that $\bar{a}_0 > 0$ in the following discussion. Using Eq. (4.9), the condition (3.5) translates to

$$\mathcal{F}_- < \bar{\beta}_4\bar{a}_0^{2n-2} < \mathcal{F}_+, \tag{4.10}$$

where $\mathcal{F}_\pm$ are defined by

$$\mathcal{F}_\pm \equiv \frac{2^{n-5}}{n^2}\left[1 - 3(2n-1)w_c \pm \sqrt{\{1 - 3(2n-1)w_c\}^2 + 32n^2(1+3w_c)\bar{a}_0^{-2}}\right]. \tag{4.11}$$

From Eqs. (2.23) and (4.5), the mass function around $r = 0$ is given by

$$M(r) = \frac{4\pi\rho_c r^3}{3[1 - 2^{1-n}(2n-1)\bar{\beta}_4\bar{a}_0^{2n}]} + \mathcal{O}(r^5). \tag{4.12}$$

To ensure that $M(r) > 0$ around the center of the star, we require the condition

$$\bar{\beta}_4\bar{a}_0^{2n} < \frac{2^{n-1}}{2n-1}, \tag{4.13}$$

which is automatically satisfied for $\bar{\beta}_4 < 0$. If $\bar{\beta}_4 > 0$, the upper limit corresponding to Eq. (4.13) leads to the divergence of the quantity f_2 in Eq. (4.9), so the condition $\bar{\beta}_4\bar{a}_0^{2n-2} < \mathcal{F}_+$ gives a tighter bound than Eq. (4.13).

The coupling $\bar{\beta}_4$ affects the decreasing rate of the pressure $P(r)$ through the function f_2, whose value in GR is given by $f_2^{\rm GR} = 4\pi(1+3w_c)/(3r_c^2)$. The difference between f_2 and $f_2^{\rm GR}$ is

$$f_2 - f_2^{\rm GR} = \frac{8\pi\bar{\beta}_4\bar{a}_0^{2n}[2^n\{4n - 1 + 3w_c(2n-1)\} - 2\bar{\beta}_4\bar{a}_0^{2n-2}\{8n^2 + \bar{a}_0^2(2n-1)^2(1+3w_c)\}]}{3[2^n - 2\bar{\beta}_4\bar{a}_0^{2n}(2n-1)]^2 r_c^2}. \tag{4.14}$$

For $\bar{\beta}_4 < 0$, the rhs of Eq. (4.14) is negative and hence $f_2 < f_2^{\rm GR}$. If the solution (4.7) is extrapolated up to the surface of the star, it is expected that the radius R_* is larger than that in GR due to the slower decrease of $P(r)$ toward 0. Since the amplitude of negative coupling is not constrained from the condition $M(r) > 0$, the radius R_* is not bounded from above. This property is different from that in cubic power-law couplings where R_* is constrained as Eq. (3.18) from the condition $M(r) > 0$.

If $\bar{\beta}_4 > 0$ and $|\bar{\beta}_4|\bar{a}_0^{2n-2} \ll 1$, then the first term in the square bracket of the numerator of Eq. (4.14) dominates over the second one, so that $f_2 > f_2^{\rm GR}$. In this regime, the radius R_* should be smaller than that in GR due to the faster decrease of $P(r)$ toward 0. For increasing $\bar{\beta}_4$ and $\bar{a}_0$, the function f_2 reaches a maximum and then it starts to decrease toward 0 (which corresponds to $\bar{\beta}_4\bar{a}_0^{2n-2} = \mathcal{F}_+$). As a function of $\bar{\beta}_4$, f_2 has the maximum value

$$f_2^{\rm max} = \frac{\pi[32n^2(1+3w_c) + \bar{a}_0^2\{1 + 3(1-2n)w_c\}^2]}{6n[4n - \bar{a}_0^2(2n-1)]r_c^2}, \tag{4.15}$$

at

$$\bar{\beta}_4 = \frac{2^{n-1}[2(2+3w_c)n - 1 - 3w_c]}{16n^2 - \bar{a}_0^2(2n-1)[1 + 3(1-2n)w_c]}\bar{a}_0^{2-2n}. \tag{4.16}$$

The coupling (4.16) is smaller than the upper limit $\bar{\beta}_4 = \mathcal{F}_+\bar{a}_0^{2-2n}$ determined by Eq. (4.10). This gives the following bound:

$$\bar{a}_0 < \bar{a}_{\rm max} \equiv \sqrt{\frac{4n}{2n-1}}. \tag{4.17}$$

The regime in which the condition $f_2 < f_2^{\rm GR}$ is satisfied is given by

$$\mathcal{F}_c \bar{a}_0^{2-2n} < \bar{\beta}_4 < \mathcal{F}_+ \bar{a}_0^{2-2n}, \tag{4.18}$$

where

$$\mathcal{F}_c \equiv \frac{2^{n-1}[2(2+3w_c)n-1-3w_c]}{8n^2+\bar{a}_0^2(2n-1)^2(1+3w_c)}. \tag{4.19}$$

To realize the slower decrease of $P(r)$ around $r=0$ relative to the GR case, we need to choose the large value of $\bar{\beta}_4 \bar{a}_0^{2n-2}$ close to $\mathcal{F}_+$. For given $\bar{\beta}_4$ and $n>1$, this amounts to choosing larger $\bar{a}_0$ close to the upper bound (4.17). Taking the limit $\bar{a}_0 \to \bar{a}_{\rm max}$, however, both $\mathcal{F}_c \bar{a}_0^{2-2n}$ and $\mathcal{F}_+ \bar{a}_0^{2-2n}$ approach the same value $(2n-1)^{n-1}/(2^{n+1}n^n)$. In this limit, the parameter space consistent with Eq. (4.18) disappears with the divergence of $f_2^{\rm max}$. Even if we consider the value $\bar{a}_0 = \bar{a}_{\rm max} - \varepsilon$, where ε is a small positive parameter, the expansions of $\mathcal{F}_c \bar{a}_0^{2-2n}$ and $\mathcal{F}_+ \bar{a}_0^{2-2n}$ in terms of ε show that two terms are equivalent up to the order of ε. Since the difference between $\mathcal{F}_c \bar{a}_0^{2-2n}$ and $\mathcal{F}_+ \bar{a}_0^{2-2n}$ appears only at the order of ε^2, the parameter space consistent with Eq. (4.18) is restricted to be very narrow. This discussion shows that, for $\bar{\beta}_4 > 0$, the function f_2 is in the range $f_2 > f_2^{\rm GR}$ for most of the parameters under consideration, which should result in smaller R_* compared to the GR case.

In the following, we will confirm the above analytic estimation by numerically solving Eqs. (2.13)–(2.15) and (2.18) with $A_1 = 0$.

B. Numerical solutions

For the numerical computation, we focus on the case of quartic vector Galileons ($n=2$). The properties of solutions in other power-law models ($n \neq 2$) are qualitatively similar to those discussed below.

In Fig. 5, we plot the mass function $M(r)$ versus r for several different values of $\bar{\beta}_4$ and $\bar{a}_0$ with the same central density ρ_c. We employ the polytropic EOS (2.34) with $\Gamma = 2.34$ and $K = 0.01$. The mass M_* and the radius R_* of the star can be identified by the point at which $M(r)$ stops increasing, e.g., $M_* \simeq 1.4\ M_\odot$ and $R_* \simeq 9.5$ km in GR ($\bar{\beta}_4 = 0$). As we analytically estimated above, the value of $M(r)$ for $\bar{\beta}_4 < 0$ is smaller than that in GR at small distances. However, as we see in case (i) of Fig. 5, the mass function in the former catches up with that in the latter at an intermediate distance inside the star, so the resulting mass M_* gets larger. Moreover, we have numerically confirmed that the negative coupling $\bar{\beta}_4$ leads to a slower decrease of the pressure $P(r)$ up to the star surface relative to the case $\bar{\beta}_4 = 0$, which results in a greater radius R_*. The case (i) in Fig. 5 shows that both R_* and M_* are larger than those in GR. When $\bar{\beta}_4 > 0$, the mass function $M(r)$ at small distances is larger than that for $\bar{\beta}_4 = 0$. This property can be seen in case (ii) of Fig. 5, but the increase of $M(r)$ stops at a smaller radius R_* because of a faster decrease of $P(r)$. Hence the mass M_* in case (ii) is smaller than that in GR.

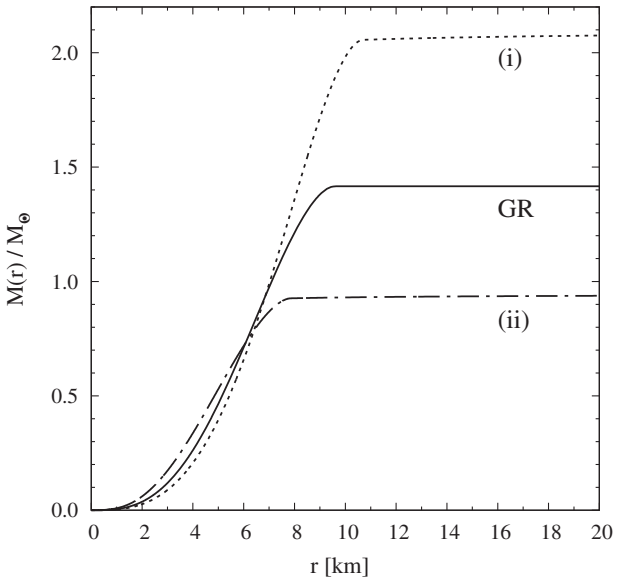

FIG. 5. The mass function $M(r)$ versus the distance r in quartic Galileons ($n=2$) for the polytropic EOS (2.34) with $\Gamma = 2.34$, $K = 0.010$, and the central density $\rho_c = 2.3 \times 10^{15}\ {\rm g \cdot cm^{-3}}$. The two curves at the top and bottom correspond to the model parameters (i) $\bar{\beta}_4 = -0.06$, $\bar{a}_0 = 1.5$, and (ii) $\bar{\beta}_4 = 0.06$, $\bar{a}_0 = 1.5$, while the solid curve corresponds to GR with $\bar{\beta}_4 = 0$, $\bar{a}_0 = 0$.

In Fig. 6, we show the mass-radius relation for the polytropic EOS with $\Gamma = 2.34$ and $K = 0.01$ in the presence of quartic Galileon couplings $\bar{\beta}_4 = -0.1$ or $\bar{\beta}_4 = 0.1$. Compared to GR, the negative coupling $\bar{\beta}_4$ leads to larger values of M_* and R_*. For this EOS, the maximum value of M_* in GR is given by $M_{\rm max} = 1.51\ M_\odot$ with the central density $\rho_c = 4.1 \times 10^{15}\ {\rm g \cdot cm^{-3}}$ and the radius $R_* = 8.48$ km. In the presence of negative $\bar{\beta}_4$, the larger maximum mass can be realized with the smaller central density. In case (c) plotted in Fig. 6, which corresponds to $\bar{\beta}_4 = -0.1$ and $\bar{a}_0 = 1.3$, the maximum mass $M_{\rm max} = 2.06\ M_\odot$ with the radius $R_* = 11.8$ km is reached at the density $\rho_c = 1.6 \times 10^{15}\ {\rm g \cdot cm^{-3}}$. If we increase either $|\bar{\beta}_4|$ or $\bar{a}_0$ further, $M_{\rm max}$ becomes larger. Indeed, the condition $M(r) > 0$ around $r = 0$ does not restrict the amplitude of negative coupling $\bar{\beta}_4$, so the mass M_* can be even larger than $3\ M_\odot$ for $\bar{\beta}_4$ close to the lower limit determined by the condition $\bar{\beta}_4 \bar{a}_0^2 = \mathcal{F}_-$.

In cases (e) and (f) depicted in Fig. 6, which correspond to $\bar{\beta}_4 > 0$, the mass M_* and the radius R_* are smaller than those in GR, independent of the detail of EOSs. In these cases the condition $f_2 > f_2^{\rm GR}$ is satisfied, so the faster decrease of $P(r)$ leads to the smaller radius R_* compared to that in GR. As shown in Fig. 5, the mass function $M(r)$ is larger than that for $\bar{\beta}_4 = 0$ in the central region of the

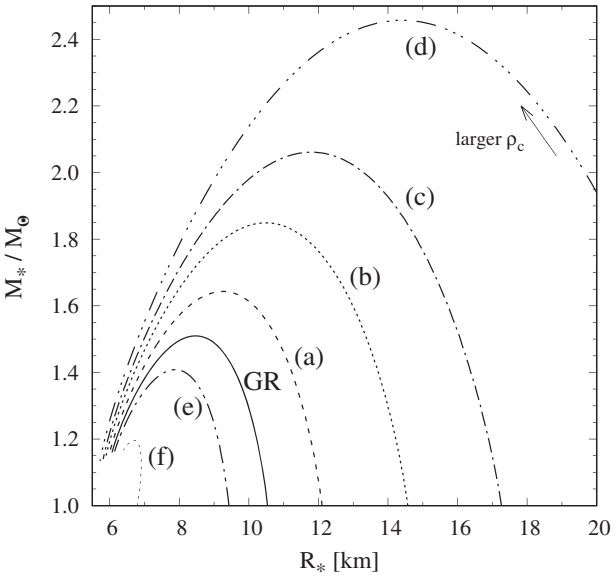

FIG. 6. Mass-radius relations in quartic Galileons for the polytropic EOS (2.34) with $\Gamma = 2.34$, $K = 0.01$. We use Eqs. (4.4)–(4.7) as the boundary conditions at the distance $r = 10^{-3} r_0$. Each curve corresponds to (a) $\bar{\beta}_4 = -0.1$, $\bar{a}_0 = 1.0$, (b) $\bar{\beta}_4 = -0.1$, $\bar{a}_0 = 1.2$, (c) $\bar{\beta}_4 = -0.1$, $\bar{a}_0 = 1.3$, (d) $\bar{\beta}_4 = -0.1$, $\bar{a}_0 = 1.4$, (e) $\bar{\beta}_4 = +0.1$, $\bar{a}_0 = 1.0$, and (f) $\bar{\beta}_4 = +0.1$, $\bar{a}_0 = 1.5$. The GR case with $\bar{\beta}_4 = 0$ and $\bar{a}_0 = 1.0$ is plotted as the solid line. With increasing ρ_c, the values of M_* and R_* shift to the direction shown as the arrow inside the figure.

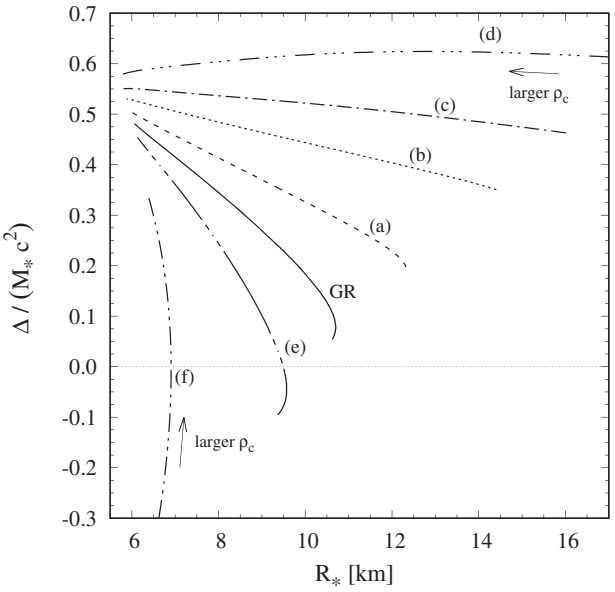

FIG. 7. The binding energy Δ normalized by $M_* c^2$ versus the radius R_* in quartic Galileons for the polytropic EOS with $\Gamma = 2.34$ and $K = 0.01$ in the range $3 \leq y_c \leq 200$. Each curve corresponds to the cases plotted in Fig. 6.

star, but the decrease of R_* induced by positive $\bar{\beta}_4$ overwhelms this effect to end up with smaller M_*. We recall that there exists the restricted parameter range (4.18) in which the condition $f_2 < f_2^{\rm GR}$ can be satisfied for $\bar{\beta}_4 > 0$. When $n = 2$, $\bar{\beta}_4 = 0.1$, and $w_c = 0.4$, for example, the bound (4.18) translates to $1.600746 < \bar{a}_0 < 1.600816$, whose parameter space is very narrow. Moreover, we find that the solutions in such a narrow parameter region are prone to numerical instabilities. Thus, the positive coupling $\bar{\beta}_4$ generally leads to the suppression of M_* and R_* in most of the parameter space with stable solutions.

The instability of the star for large positive values of $\bar{\beta}_4 \bar{a}_0^2$ close to $\mathcal{F}_+$ can also be confirmed by computing the binding energy Δ defined by Eq. (3.20). In Fig. 7, we show $\Delta/(M_* c^2)$ versus the radius R_* for $\Gamma = 2.34$ and $K = 0.01$ with several different values of $\bar{\beta}_4$ and $\bar{a}_0$. When $\bar{\beta}_4 < 0$, the binding energy is always positive, so the star is gravitationally bound. If $\bar{\beta}_4 > 0$, Δ can be negative in the region of small central density ρ_c. In cases (e) and (f) shown in Fig. 7, Δ is negative for $\rho_c < 1.2 \times 10^{15}$ g $\cdot$ cm^{-3} and $\rho_c < 8.2 \times 10^{15}$ g $\cdot$ cm^{-3}, respectively, so that the region of instability tends to be larger for $\bar{\beta}_4 \bar{a}_0^2$ approaching the upper limit $\mathcal{F}_+$. Thus, for $\bar{\beta}_4 > 0$, it is difficult to realize the stable configuration of the star with M_* and R_* larger than those in GR.

V. INTRINSIC VECTOR-MODE COUPLINGS

Finally, we investigate the relativistic star solutions in the presence of intrinsic vector-mode couplings given by

$$G_2 = -2g_4(X)F, \quad g_5 = g_5(X), \quad G_6 = G_6(X), \tag{5.1}$$

with $G_4 = 1/(16\pi G)$, where $g_4(X)$ is a function of X, and $F = hA_0'^2/(2f)$ on the background (2.9). From Eq. (2.16), it follows that

$$A_0'^2[\{r^2 g_{4,X} + (3h-1)G_{6,X}\}A_1 - 2rg_5 + 2hrg_{5,X}A_1^2 - G_{6,XX}h^2A_1^3] = 0. \tag{5.2}$$

We can write Eq. (2.15) in the following form:

$$\alpha_1 A_0'' + \alpha_2 A_0' + \alpha_3 A_0'^2 = 0, \tag{5.3}$$

where $\alpha_{1,2,3}$ are functions containing A_0, A_1, A_1', f, h, f', h' and g_4, g_5, G_6 as well as their X-derivatives. The explicit expression of the coefficient α_1 is given by

$$\alpha_1 = (2g_4 - 1)r^2 + 4hrg_5A_1 - 2h^2A_1^2G_{6,X} + 2(h-1)G_6. \tag{5.4}$$

From Eq. (5.2), there is a branch characterized by $A_0'(r) = 0$, that is

$$A_0(r) = \text{constant}, \tag{5.5}$$

which is consistent with Eq. (5.3).

There exist other branches where the terms in the square brackets of Eq. (5.2) vanish, which can give rise to a nonvanishing longitudinal component A_1. Even in such cases, the temporal vector component needs to obey the regular boundary condition $A_0'(0) = 0$ at the center of the star. Then, we obtain $\alpha_1 A_0''(0) = 0$ from Eq. (5.3), so that $A_0''(0) = 0$ for $\alpha_1 \neq 0$. This means that, when we integrate Eq. (5.3) from $r = 0$ with the boundary condition $A_0'(0) = 0$, the derivative $A_0'(r)$ remains 0 for arbitrary r. Then, provided that $\alpha_1 \neq 0$, we end up with the solution (5.5) even for the branches other than $A_0'(r) = 0$ in Eq. (5.2). Substituting the solution $A_0'(r) = 0$ into Eqs. (2.13) and (2.14), it follows that

$$\frac{h'}{r} + \frac{h-1}{r^2} = -\frac{8\pi G\rho}{c^2}, \tag{5.6}$$

$$\frac{h}{f}\frac{f'}{r} + \frac{h-1}{r^2} = \frac{8\pi G P}{c^4}, \tag{5.7}$$

which are exactly the same as Eqs. (2.21) and (2.22) in GR, respectively. This shows that the intrinsic vector-mode couplings do not give rise to any modifications to the metric components f and h. The TOV equation also holds in the same form as Eq. (2.25). Thus, for a given EOS, the solutions to f, h, P, ρ are the same as those in GR with $A_0(r) =$ constant. Requiring the smooth matching of the metric and vector field at the surface, Eq. (5.5) remains the solution outside the star with the exterior metric given by the Schwarzschild solution (2.30).

The above property is in stark contrast with that in cubic and quartic couplings where the differential equation corresponding to Eq. (5.3) contains the A_0-dependent terms which are not multiplied by the powers of A_0'. As we discussed in Secs. III and IV, the existence of such terms leads to the variation of $A_0(r)$ for $r > 0$. We also note that the presence of mass contribution m^2X to G_2 gives rise to the terms m^2A_1 and m^2A_0 to Eqs. (5.2) and (5.3), respectively, so the general solution to $A_0(r)$ is different from Eq. (5.5).

In summary, the intrinsic vector-mode couplings (5.1) only lead to the metric components in GR with the trivial temporal vector component (5.5) as the unique solution for relativistic stars, indicating no-hair properties unlike the BH solutions studied in Refs. [59,60]. This no-hair property of relativistic stars is intrinsically related to the regular boundary condition $A_0'(r) = 0$ at the center of the star together with the peculiar structure of the differential Eq. (5.3). The result in this section holds irrespective of the choice of the coupling functions and the detail of EOSs.

VI. CONCLUSIONS

In this paper, we studied how the mass-radius relation of relativistic stars is modified in generalized Proca theories. In these theories there exists a $U(1)$-breaking vector field with derivative couplings, which leads to the propagation of fifth forces. On the weak gravitational background in the Solar System, it is known that such fifth forces can be suppressed by derivative self-interactions under the operation of the Vainshtein mechanism [49,50]. On the other hand, the deviation from GR can manifest itself in the strong gravitational regime like BHs [59,60]. Indeed, there exist a bunch of hairy BH solutions in generalized Proca theories. Our interest in this paper was to show how the new "hair" induced by vector-field derivative couplings affects the configuration of relativistic stars.

In Sec. III we considered the cubic power-law derivative coupling (3.1) including the vector Galileon ($n = 1$) as a specific case. In these models, the vector field has a nonvanishing longitudinal mode A_1 related to the temporal component A_0 according to Eq. (3.2). Imposing the regularity of metrics, pressure, density, and the vector field at the center of the star ($r = 0$), we derived the analytic solutions (3.8)–(3.11) around $r = 0$. As we see in Eq. (3.11), the negative coupling constant β_3 leads to a slower decrease of the matter pressure $P(r)$. This slower decrease continues up to the star surface, so the resulting radius R_* for $\beta_3 < 0$ tends to be larger than that in GR. We also showed that the amplitude of negative coupling β_3 is constrained as Eq. (3.16) from the demand $M(r) > 0$ around $r = 0$. This limits the maximum radius reached by the cubic coupling; see Eq. (3.18). These properties hold independently of the EOS of relativistic stars.

To compute the mass M_* and the radius R_* of relativistic stars precisely, we numerically solved Eqs. (2.13)–(2.16) for the cubic Galileon coupling $G_3 = \beta_3 X$ by employing the polytropic EOS (2.34) with $\Gamma = 2.34$. We confirmed that the negative coupling β_3 gives rise to R_* larger than in the case $\beta_3 = 0$. Although the mass function $M(r)$ is suppressed by negative β_3 around $r = 0$, the increase of R_* overwhelms this decrease to realize the mass M_* greater than that in GR. As we observe in Fig. 2, the maximum mass $M_{\rm max}$ increases for a larger temporal vector component a_0 at $r = 0$ and for an increasing amplitude of negative coupling β_3. For $\beta_3 > 0$, both M_* and R_* are smaller than those in GR. Moreover, the models with large positive values of β_3 and a_0 are prone to instabilities associated with a negative gravitational binding energy Δ in the low-density regime.

In Sec. IV we studied the effect of quartic power-law couplings (4.1) on the configuration of relativistic stars by considering the branch $A_1 = 0$. Again, the negative coupling β_4 leads to the larger mass M_* and the larger radius R_* relative to those in GR. The difference from cubic derivative interactions is that the amplitude of negative β_4 is not constrained from the condition $M(r) > 0$. For $\beta_4 > 0$ we found that both M_* and R_* are smaller than those in GR for most of the parameter space. The solutions are also subject to instabilities in the low-density regime with increasing values of β_4 and a_0. This is not the case for

negative β_4 where the necessary condition for the dynamical stability is satisfied.

In Sec. V we showed that the intrinsic vector-mode couplings (5.1) give rise to the same solutions as those in GR with the constant value of A_0. This is attributed to the peculiar structure of the differential equation (5.3) as well as the regular boundary condition $A_0' = 0$ at $r = 0$. Thus, the intrinsic vector modes do not modify the radius and mass of relativistic stars in GR.

There are several issues we did not address in this paper. We adopted the polytropic EOS (2.34) with $\Gamma = 2.34$ to compute the mass and radius of relativistic stars, but for comparison with the observational data of NSs, we need to extend the analysis to more realistic EOSs by taking into account nuclear interactions and the composition of each layer of NSs. It is also possible to include the rotation of NSs in our analysis along the lines of Ref. [67] and investigate the existence of EOS-independent relations [18] useful to test generalized Proca theories with NSs further. Although we have confirmed that most of the solutions obtained in this paper are gravitationally bound, the analysis of dynamical stabilities against odd- and even-parity perturbations may provide further constraints on couplings in generalized Proca theories. With this perturbative analysis on the spherically symmetric background, we should also be able to derive the local propagation speed c_g of gravitational waves around NSs. If the vector-field derivative couplings studied in this paper are also responsible for today's cosmic acceleration, the recent GW170817 bound of c_g [6] on the cosmological background will provide tight constraints on quartic derivative couplings. These interesting issues will be left for future works.

ACKNOWLEDGMENTS

We thank Lavinia Heisenberg for useful discussions. R. K. is supported by the Grant-in-Aid for Young Scientists B of the JSPS, Grant No. 17K14297. M. M. is supported by FCT-Portugal through Grant No. SFRH/BPD/88299/2012. S. T. is supported by the Grant-in-Aid for Scientific Research Fund of the JSPS, Grant No. 16K05359, and the MEXT KAKENHI Grant-in-Aid for Scientific Research on Innovative Areas "Cosmic Acceleration," Grant No. 15H05890.

APPENDIX: COEFFICIENTS IN THE GRAVITATIONAL EQUATIONS OF MOTION

The coefficients $c_{1,2,\ldots,19}$ in Eqs. (2.13) and (2.14) are given by

$$
\begin{aligned}
c_1 &= -A_1 X G_{3,X},\\
c_2 &= -2G_4 + 4(X_0 + 2X_1)G_{4,X} + 8X_1 X G_{4,XX},\\
c_3 &= -A_1(3hX_0 + 5hX_1 - X)G_{5,X} - 2hA_1 X_1 X G_{5,XX},\\
c_4 &= G_2 - 2X_0 G_{2,X} - \frac{h}{f}(A_0 A_1 A_0' + 2fXA_1')G_{3,X} - \frac{hA_0'^2(1 + 2G_{2,F})}{2f},\\
c_5 &= -4hA_1 X_0 G_{3,X} - 4h^2 A_1 A_1' G_{4,X} + \frac{8h}{f}(A_0 X_1 A_0' - fhA_1 X A_1')G_{4,XX} + \frac{2h^2}{f}A_1 A_0'^2(g_5 + 2X_0 g_{5,X}),\\
c_6 &= 2(1-h)G_4 + 4(hX - X_0)G_{4,X} + 8hX_0 X_1 G_{4,XX} - \frac{h}{f}[(h-1)A_0 A_1 A_0' + 2f(3hX_1 + hX_0 - X)A_1']G_{5,X}\\
&\quad - \frac{2h^2 X_1}{f}(A_0 A_1 A_0' + 2fXA_1')G_{5,XX} + \frac{hA_0'^2}{f}[(h-1)G_6 + 2(hX - X_0)G_{6,X} + 4hX_0 X_1 G_{6,XX}],\\
c_7 &= -G_2 + 2X_1 G_{2,X} - \frac{h}{f}A_0 A_1 A_0' G_{3,X} + \frac{hA_0'^2(1 + 2G_{2,F})}{2f},\\
c_8 &= 4hA_1 X_1 G_{3,X} + \frac{4h}{f}A_0 A_0'(G_{4,X} + 2X_1 G_{4,XX}) - \frac{2h^2}{f}A_1 A_0'^2(3g_5 + 2X_1 g_{5,X}),\\
c_9 &= 2(h-1)G_4 - 4(2h-1)X_1 G_{4,X} - 8hX_1^2 G_{4,XX} - \frac{h}{f}A_0 A_1 A_0'[(3h-1)G_{5,X} + 2hX_1 G_{5,XX}]\\
&\quad - \frac{h}{f}A_0'^2[(3h-1)G_6 + 2(6h-1)X_1 G_{6,X} + 4hX_1^2 G_{6,XX}].
\end{aligned}
$$

[1] A. G. Riess *et al.* (Supernova Search Team), Astron. J. **116**, 1009 (1998); S. Perlmutter *et al.* (Supernova Cosmology Project Collaboration), Astrophys. J. **517**, 565 (1999).

[2] D. N. Spergel *et al.* (WMAP Collaboration), Astrophys. J. Suppl. Ser. **148**, 175 (2003); P. A. R. Ade *et al.* (Planck Collaboration), Astron. Astrophys. **571**, A16 (2014).

[3] A. I. Vainshtein, Phys. Lett. **39B**, 393 (1972).

[4] J. Khoury and A. Weltman, Phys. Rev. Lett. **93**, 171104 (2004).

[5] B. P. Abbott *et al.* (LIGO Scientific and Virgo Collaborations), Phys. Rev. Lett. **116**, 061102 (2016); **116**, 241103 (2016); **118**, 221101 (2017); **119**, 141101 (2017).

[6] B. P. Abbott *et al.* (LIGO Scientific and Virgo and Fermi-GBM and INTEGRAL Collaborations), Astrophys. J. Lett. **848**, L13 (2017).

[7] E. Berti, V. Cardoso, and C. M. Will, Phys. Rev. D **73**, 064030 (2006); P. Pani, V. Cardoso, and L. Gualtieri, Phys. Rev. D **83**, 104048 (2011); V. Cardoso, E. Franzin, A. Maselli, P. Pani, and G. Raposo, Phys. Rev. D **95**, 084014 (2017).

[8] K. Yagi, L. C. Stein, N. Yunes, and T. Tanaka, Phys. Rev. D **85**, 064022 (2012); K. Yagi, N. Yunes, and T. Tanaka, Phys. Rev. Lett. **109**, 251105 (2012); M. Okounkova, L. C. Stein, M. A. Scheel, and D. A. Hemberger, Phys. Rev. D **96**, 044020 (2017).

[9] S. L. Shapiro and S. A. Teukolsky, *Black Holes, White Dwarfs and Neutron Stars* (Wiley-VCH, Weinheim, 1983).

[10] J. M. Lattimer and M. Prakash, Science **304**, 536 (2004).

[11] F. Ozel and P. Freire, Annu. Rev. Astron. Astrophys. **54**, 401 (2016).

[12] T. Clifton, P. G. Ferreira, A. Padilla, and C. Skordis, Phys. Rep. **513**, 1 (2012).

[13] T. Damour and G. Esposito-Farese, Phys. Rev. Lett. **70**, 2220 (1993); Phys. Rev. D **54**, 1474 (1996).

[14] T. Harada, Phys. Rev. D **57**, 4802 (1998).

[15] J. Novak, Phys. Rev. D **58**, 064019 (1998).

[16] H. O. Silva, C. F. B. Macedo, E. Berti, and L. C. B. Crispino, Classical Quantum Gravity **32**, 145008 (2015).

[17] P. C. C. Freire, N. Wex, G. Esposito-Farèse, J. P. W. Verbiest, M. Bailes, B. A. Jacoby, M. Kramer, I. H. Stairs, J. Antoniadis, and G. H. Janssen, Mon. Not. R. Astron. Soc. **423**, 3328 (2012).

[18] D. D. Doneva and G. Pappas, arXiv:1709.08046.

[19] A. Nicolis, R. Rattazzi, and E. Trincherini, Phys. Rev. D **79**, 064036 (2009); C. Deffayet, G. Esposito-Farese, and A. Vikman, Phys. Rev. D **79**, 084003 (2009); C. Deffayet, X. Gao, D. A. Steer, and G. Zahariade, Phys. Rev. D **84**, 064039 (2011); T. Kobayashi, M. Yamaguchi, and J. Yokoyama, Prog. Theor. Phys. **126**, 511 (2011).

[20] G. W. Horndeski, Int. J. Theor. Phys. **10**, 363 (1974).

[21] A. Lehebel, E. Babichev, and C. Charmousis, J. Cosmol. Astropart. Phys. 07 (2017) 037.

[22] L. Hui and A. Nicolis, Phys. Rev. Lett. **110**, 241104 (2013).

[23] T. P. Sotiriou and S. Y. Zhou, Phys. Rev. Lett. **112**, 251102 (2014).

[24] T. P. Sotiriou and S. Y. Zhou, Phys. Rev. D **90**, 124063 (2014).

[25] E. Babichev and C. Charmousis, J. High Energy Phys. 08 (2014) 106.

[26] T. Kobayashi and N. Tanahashi, Prog. Theor. Exp. Phys. **2014**, 073E02 (2014).

[27] C. Charmousis, T. Kolyvaris, E. Papantonopoulos, and M. Tsoukalas, J. High Energy Phys. 07 (2014) 085.

[28] E. Babichev, C. Charmousis, A. Lehebel, and T. Moskalets, J. Cosmol. Astropart. Phys. 09 (2016) 011.

[29] M. Rinaldi, Phys. Rev. D **86**, 084048 (2012).

[30] A. Anabalon, A. Cisterna, and J. Oliva, Phys. Rev. D **89**, 084050 (2014).

[31] M. Minamitsuji, Phys. Rev. D **89**, 064017 (2014).

[32] A. Cisterna, T. Delsate, and M. Rinaldi, Phys. Rev. D **92**, 044050 (2015).

[33] A. Cisterna, T. Delsate, L. Ducobu, and M. Rinaldi, Phys. Rev. D **93**, 084046 (2016).

[34] A. Maselli, H. O. Silva, M. Minamitsuji, and E. Berti, Phys. Rev. D **93**, 124056 (2016).

[35] E. Babichev, K. Koyama, D. Langlois, R. Saito, and J. Sakstein, Classical Quantum Gravity **33**, 235014 (2016).

[36] F. G. Lopez Armengol and G. E. Romero, Gen. Relativ. Gravit. **49**, 27 (2017); P. Brax, A. C. Davis, and R. Jha, Phys. Rev. D **95**, 083514 (2017).

[37] Y. Ali-Haimoud and Y. Chen, Phys. Rev. D **84**, 124033 (2011); C. Deliduman, K. Y. Eksi, and V. Keles, J. Cosmol. Astropart. Phys. 05 (2012) 036; M. Orellana, F. Garcia, F. A. Teppa Pannia, and G. E. Romero, Gen. Relativ. Gravit. **45**, 771 (2013); A. Ganguly, R. Gannouji, R. Goswami, and S. Ray, Phys. Rev. D **89**, 064019 (2014); K. V. Staykov, D. D. Doneva, S. S. Yazadjiev, and K. D. Kokkotas, J. Cosmol. Astropart. Phys. 10 (2014) 006.

[38] S. H. Hendi, G. H. Bordbar, B. Eslam Panah, and S. Panahiyan, J. Cosmol. Astropart. Phys. 07 (2017) 004.

[39] L. Heisenberg, J. Cosmol. Astropart. Phys. 05 (2014) 015.

[40] G. Tasinato, J. High Energy Phys. 04 (2014) 067; Classical Quantum Gravity **31**, 225004 (2014).

[41] E. Allys, P. Peter, and Y. Rodriguez, J. Cosmol. Astropart. Phys. 02 (2016) 004; E. Allys, J. P. Beltran Almeida, P. Peter, and Y. Rodriguez, J. Cosmol. Astropart. Phys. 09 (2016) 026.

[42] J. B. Jimenez and L. Heisenberg, Phys. Lett. B **757**, 405 (2016).

[43] G. W. Horndeski, J. Math. Phys. (N.Y.) **17**, 1980 (1976).

[44] L. Heisenberg, R. Kase, and S. Tsujikawa, Phys. Lett. B **760**, 617 (2016).

[45] R. Kimura, A. Naruko, and D. Yoshida, J. Cosmol. Astropart. Phys. 01 (2017) 002.

[46] A. De Felice, L. Heisenberg, R. Kase, S. Mukohyama, S. Tsujikawa, and Y. l. Zhang, J. Cosmol. Astropart. Phys. 06 (2016) 048; L. Heisenberg, R. Kase, and S. Tsujikawa, J. Cosmol. Astropart. Phys. 11 (2016) 008.

[47] A. De Felice, L. Heisenberg, R. Kase, S. Mukohyama, S. Tsujikawa, and Y. l. Zhang, Phys. Rev. D **94**, 044024 (2016).

[48] S. Nakamura, R. Kase, and S. Tsujikawa, Phys. Rev. D **95**, 104001 (2017); A. De Felice, L. Heisenberg, and S. Tsujikawa, Phys. Rev. D **95**, 123540 (2017).

[49] A. De Felice, L. Heisenberg, R. Kase, S. Tsujikawa, Y. l. Zhang, and G. B. Zhao, Phys. Rev. D **93**, 104016 (2016).

[50] S. Nakamura, R. Kase, and S. Tsujikawa, Phys. Rev. D **96**, 084005 (2017).

[51] J. D. Bekenstein, Phys. Rev. Lett. **28**, 452 (1972).

[52] G. W. Horndeski, Phys. Rev. D **17**, 391 (1978).

[53] J. Chagoya, G. Niz, and G. Tasinato, Classical Quantum Gravity **33**, 175007 (2016).
[54] Z. Y. Fan, J. High Energy Phys. 09 (2016) 039.
[55] M. Minamitsuji, Phys. Rev. D **94**, 084039 (2016).
[56] A. Cisterna, M. Hassaine, J. Oliva, and M. Rinaldi, Phys. Rev. D **94**, 104039 (2016).
[57] J. Chagoya, G. Niz, and G. Tasinato, Classical Quantum Gravity **34**, 165002 (2017).
[58] E. Babichev, C. Charmousis, and M. Hassaine, J. High Energy Phys. 05 (2017) 114.
[59] L. Heisenberg, R. Kase, M. Minamitsuji, and S. Tsujikawa, Phys. Rev. D **96**, 084049 (2017).
[60] L. Heisenberg, R. Kase, M. Minamitsuji, and S. Tsujikawa, J. Cosmol. Astropart. Phys. 08 (2017) 024.
[61] J. Chagoya and G. Tasinato, J. Cosmol. Astropart. Phys. 01 (2018) 046.
[62] F. Filippini and G. Tasinato, J. Cosmol. Astropart. Phys. 01 (2018) 033.
[63] Z. Y. Fan, Eur. Phys. J. C **78**, 65 (2018).
[64] T. W. Baumgarte and S. L. Shapiro, *Numerical Relativity: Solving Einstein's Equations on the Computer* (Cambridge University Press, Cambridge, England, 2010).
[65] J. S. Read, B. D. Lackey, B. J. Owen, and J. L. Friedman, Phys. Rev. D **79**, 124032 (2009).
[66] M. S. R. Delgaty and K. Lake, Comput. Phys. Commun. **115**, 395 (1998).
[67] J. B. Hartle, Astrophys. J. **150**, 1005 (1967); J. B. Hartle and K. S. Thorne, Astrophys. J. **153**, 807 (1968).